Chemical Engineering Faculty Publications   Chemical Engineering

2011

Hydration Repulsion Effects of the Formation of Supported Lipid Bylayers

Selver Ahmed

Rajesh Raman Madathingal

See next page for additional authors

Follow this and additional works at: https://digitalcommons.uri.edu/che_facpubs

Part of the Chemical Engineering Commons

Authors

Selver Ahmed, Rajesh Raman Madathingal, Stephanie L. Wunder, Yanjing Chen, and Geoffrey D. Bothun

Soft Matter

PAPER

Hydration repulsion effects on the formation of supported lipid bilayers

Selver Ahmed,[a] **Rajesh Raman Madathingal,**[a] **Stephanie L. Wunder,**[*a] **Yanjing Chen**[b] **and Geoffrey Bothun**[b]

When zwitterionic lipids fuse onto substrates such as silica (SiO_2), the water of hydration between the two approaching surfaces must be removed, giving rise to an effective hydration repulsion. Removal of water around the polar headgroups of the lipid and the silanols (SiOH) of SiO_2 allows supported lipid bilayer (SLB) formation, although an interstitial water layer remains between the lipid and surface. The importance of hydration repulsion in SLB formation is demonstrated by monitoring fusion of zwitterionic lipids onto silica (SiO_2) nanoparticles heat treated to control the silanol group (SiOH) density and thus the amount of bound water. SLB formation, observed by cryo-TEM and nano-differential scanning calorimetry, was found to be slower for the more hydrated surfaces. Although the SiOH density decreased with increasing heat treatment temperature, ζ-potentials were the same for all the SiO_2. This arose since at the pH = 8 of the experiments, only isolated silanols, with a $pK_a = 4.9$, and not hydrogen bonded silanols, with a $pK_a = 8.5$, were dissociated/charged.[1] Since there were no differences in double layer forces between the SUVs and SiO_2, which are the largest and most important interactions determining lipid fusion onto surfaces,[2,3] the slower rate of SLB formation of DMPC onto SiO_2 nanoparticles with higher silanol densities and more bound water was therefore attributed to greater hydration repulsion of the more hydrated nanoparticles. For SiO_2 heated to 1000 °C, with only a few isolated silanols, little adsorbed water and many hydrophobic Si–O–Si groups, particle aggregation occurred and lipid sheaths formed around the nanoparticle aggregates.

Introduction

Supported lipid bilayers (SLBs) on nanoparticles are of importance as a method of biofunctionalizing solid surfaces for drug delivery and can provide a platform to investigate membrane proteins. They have been formed on micron sized spherical[4] and nanoparticle[5–7] surfaces, and been investigated by molecular dynamics (MD) simulations.[8] SLBs can be formed on planar and curved surfaces by the fusion of small unilamellar vesicles (SUVs)[9] on a variety of inorganic and organic supports. Fusion can occur by a process of adsorption and rupture, or by a single rupture step, and can depend on factors such as the ionic strength of the medium, type of buffer and solid support.[10] While critical densities of SUVs can be required for fusion onto planar surfaces, vesicles appear to rupture one by one on SiO_2 nanoparticles.[5]

The effects of nanotopography of the substrate[11] and the substrate type[12] have been investigated by techniques such as quartz crystal microbalance with dissipation monitoring (QCM-D), where simultaneous measurements of the shift in frequency and the change in energy dissipation provide information on whether intact vesicle adsorption or vesicle fusion occurs. For zwitterionic lipids, only intact vesicles adsorb onto oxidized gold,[13,14] oxidized platinum[14] and TiO_2[14] solid supports, and in the low coverage regime where there is only intact adsorption, the flattening deformation due to collapse of the SUVs was much larger on SiO_2. Supported lipid bilayer formation occurs for SiO_2 and Si_3N_4 at higher coverage.[13,14] Although the most common inorganic support is silica (SiO_2), SLBs also form on borosilicate glass, silicon wafers, mica,[15,16] TiO_2 (rutile),[17] and $SrTiO_3$ single crystals[17] (although this has been suggested to be due to SiO_2 impurities[18]). In the case of Al_2O_3, deposition does not occur *via* a vesicle rupture process but SLBs can be formed by bubble collapse deposition.[19] The difference between SiO_2 and TiO_2 was attributed to the higher charge density of the former, due to its lower isoelectric point.[20] SLBs also form on planar polymer supports.[21,22]

Although the substrate itself affects bilayer formation, there are water layers on both the lipid and substrate that must be removed before a SLB can be formed. Not all of the water is removed, since after formation of the SLBs on silica substrates the lipid bilayer is separated from the SiO_2 support by a water layer 1.5–2.0 nm thick.[4,23] The organization of water on these surfaces may play a role in the adsorption/fusion process of lipids to form SLBs. In particular, as the two surfaces approach each other, the water of hydration must be removed from the polar headgroups of the lipid[24] and the surface water on the inorganic substrate, giving rise to an effective hydration repulsion,[25] which

[a] Department of Chemistry, Temple University, 1901 N 13th St, Beury Hall, Philadelphia, PA, 19122, USA. E-mail: slwunder@temple,edu
[b] Department of Chemical Engineering, University of Rhode Island, 16 Greenhouse Road, Crawford Hall, Kingston, RI, 02881, USA

can be affected by the nature of the water layers on the lipid and inorganic surfaces. In the case of hydrophilic planar surfaces, phospholipid bilayers spread by sliding over surfaces with a thin lubricating water film.[26]

NMR and molecular dynamics (MD) simulations of water around fully hydrated DMPC showed both a more mobile, clathrate like hydration shell of *ca.* 5–6 hydrogen-bonded water around the positively charged $N(CH_3)$ choline moiety and "frozen", less mobile, hydrogen bonded water (1–2 water molecules) with the oxygen of the phosphate.[27,28] Dynamic AFM studies of SLBs of 1,2-dipalmitoyl-*sn*-glycero-3-phosphocholine (DPPC) and 1,2-dioleoyl-*sn*-glycero-3-phosphocholine (DOPC) phospholipids showed that in the gel phase, up to 5 ordered water layers (1–3 layers more frequently observed) with spacings of *ca.* 0.29 ± 0.6 nm each between the carbon nanotube tip and the SLB could be successively removed; the layers closer to the lipid required more force to remove. Whether the structured water arose from inherent hydration layers around the lipid and/or tip or from induced confinement between the two could not be determined.[29] Molecular dynamics simulations indicated that one or two ordered water layers extended from the DPPC headgroup.[30]

Water is believed to have an organized structure with perturbations compared with bulk water about 1.0–1.5 nm from a mineral interface.[31,32] Up to seven confined water layers with spacings of 0.252 ± 0.048 nm, roughly the diameter of a water molecule, could be measured on a mica surface by off-resonance AFM, with dynamics slowed down as the confining separation was reduced.[33] The stable molecular water layers on hydrophilic silica[32] were suggested to be responsible for the hydration repulsion that has been shown to exist below 5 nm from the silica surface.[34] Thus, the energy penalty for removing water layers from both the lipid headgroup and inorganic surface can affect the rate of SLB formation.

Here we investigate the effects of surface water and silanol density of nominal 100 nm SiO_2 nanoparticles on the formation of supported lipid bilayers from 1,2-dimyristoyl-*sn*-glycero-3-phosphocholine (DMPC) small unilamellar vesicles (SUVs). The silanol densities were varied by heat (600 °C and 1000 °C) and piranha treatments and the nanoparticles characterized by dynamic light scattering (DLS), ζ-potential measurements, transmission electron microscopy (TEM), FTIR spectroscopy and thermogravimetric analysis (TGA). Unexpectedly, the kinetics of formation of SLBs were faster on nanoparticles heated to 600 °C than on fully hydroxylated ("as-is") SiO_2 nanoparticles. This was associated with a higher amount of bound water on the fully hydroxylated SiO_2. The increased affinity of the SUVs for the nanoparticles with less adsorbed water was hypothesized to be due to the different structures of the interfacial water layers on the nanoparticles. Both nanoparticles were suggested to have 1–2 monolayers of an ordered "ice-like" water layer that was hydrogen bonded to the SiOH groups, with a greater amount of disordered water around the "as-is" nanoparticles. Since the ζ-potentials of the nanoparticles were all the same (-45 ± 5 mV), indicating similar electrostatic interactions between the SUVs and the nanoparticles, the decreased affinity/fusability of the SUVs for the fully hydroxylated "as-is" SiO_2 was attributed to greater hydration repulsion between them, due to the necessity of removing more disordered

water from the more hydrated SiO_2. The SiO_2 heat treated to 1000 °C had so few SiOH groups that hydrophobic clustering of the nanoparticles occurred.

Experimental

Materials

1,2-Dimyristoyl-*sn*-glycero-3-phosphocholine (DMPC, 14 : 0 PC) was obtained from Avanti Polar Lipids (Alabaster, AL) and used without further purification. Dry colloidal silica beads with 100 nm nominal size, prepared by the Stöber process with densities of 2.0 g cm^{-3} (reported by manufacturer) were purchased from Alfa Aesar Lancaster (Ward Hill, MA) and were used as received or after thermal and/or piranha treatment. SiO_2 nanoparticles in suspension, with nominal 100 nm diameters, densities of 2.4 g cm^{-3} (reported by manufacturer) and prepared by a water glass process, were a gift from Nissan Chemical America (Houston, TX). All solutions/suspensions were prepared with HPLC grade water and chloroform, purchased from Fisher Chemicals (Fairlawn, NJ), as was the $H_2SO_4 : H_2O_2$ (70 : 30) used to make the piranha solution. A 0.1 M, pH 8.0 buffer was made from $Na_2HPO_4 \cdot 7H_2O$ and $NaH_2PO_4 \cdot H_2O$ (PBS) and 75 mM NaCl. An Avanti Mini-Extruder from Avanti Polar Lipids was used for extrusion of the lipids, using 50 nm polycarbonate filters.

Thermal/piranha modification of SiO_2

The SiO_2 described as "as is" was used from the supplier as received. The "as is" SiO_2 was thermally modified by heat treatment at 600 and 1000 °C for 7–8 hours. Thermally modified beads were further heated in piranha solution at 100 °C for 2–3 hours, and rinsed with distilled water until a pH of 7.0 was achieved. The "as-is", "as-is" + piranha, 600 °C and 600 °C + piranha SiO_2 could all be dispersed in buffer. Not all of the 1000 °C or 1000 °C + piranha SiO_2 went into suspension. Only the material that was in suspension was used for subsequent use and characterization. The amount that did redisperse was obtained by centrifuging out the non-dispersed beads and measuring (by TGA) the amount of SiO_2 in the supernatant; this weight percent was used to calculate the weight of lipid required for bilayer coverage.

Preparation of supported lipid bilayers

Appropriate amounts of lipid were dissolved in chloroform. Dry lipid films were formed after evaporation of the solutions under a stream of nitrogen and then in a vacuum oven overnight to remove any residual solvent. The lipid film was then redispersed in buffer and incubated at a temperature (*ca.* 50 °C) above the T_m of the DMPC for a minimum of 2 hours with periodic shaking to form hydrated multilamellar vesicles (MLVs). Small unilamellar vesicles (SUVs) were obtained from MLVs by subjecting them to 5 freeze/thaw cycles followed by extrusion using a polycarbonate filter with a pore size of 50 nm. Approximately 1 ml of a 5–10 mg ml^{-1} lipid solution was passed back and forth for up to 50 times. Although a clear solution was obtained after 20 passes, the vesicles became more monodisperse as the number of passes increased (as determined by dynamic light scattering data, see

below), and which had an average diameter of 60 nm. Assuming no loss of lipid during the extrusion process, additional buffer was added to the extrusion product to yield vesicle solutions of ~2 mg ml^{-1} lipid. The dry silica particles were dispersed in buffer at a concentration of 2–4 mg ml^{-1} and were sonicated for 1 hour in order to separate and prepare homogeneous colloidal solutions. The Nissan nanoparticles, which were already dispersed, were diluted in buffer to prepare the necessary concentrations.

Adsorption of the vesicles onto the nanobeads was accomplished by addition of the SiO$_2$ dispersions to the vesicle solutions held above T_m. The amount of lipid required to achieve single bilayer coverage was calculated using the surface area occupied by the lipid headgroup (0.59 nm^2 for DMPC[35]) and the total surface area of the nanoparticles, with the assumption that the latter was a planar surface; values for the density of 2.0 g cm^{-3} and 2.4 g cm^{-3} were used for the Lancaster and Nissan SiO$_2$, respectively. The amount of lipid required for single bilayer coverage of the nanoparticles is achieved when the surface area of the SUVs (SA$_{SUV}$) was equal to the surface area of the SiO$_2$ (SA$_{SiO_2}$) SA$_{SUV}$/SA$_{SiO_2}$ = 1; other coverages will be referred to as fractions or multiples of this amount. For SiO$_2$ heat treated to 1000 °C, not all of the SiO$_2$ could be redispersed; only the fraction that was dispersed was used for the calculations.

For nano-DSC measurements, mixtures with variable SA$_{SUV}$/SA$_{SiO_2}$ ratios were incubated at 50 °C for 2 h, cooled to RT and stored at 4 °C. For time dependent measurements, mixtures with ratios of SA$_{SUV}$/SA$_{SiO_2}$ = 1.5 were prepared at RT and run immediately at 30 °C (see nano-DSC below). The excess lipid was used to stabilize the suspensions; we have previously shown that flocculation/precipitation of SLBs could be prevented by addition of excess SUVs.[7] TGA samples were prepared with excess SUVs (SA$_{SUV}$/SA$_{SiO_2}$ = 2–5), incubated at 50 °C for 2 h and cooled to RT. They were then centrifuged at 3900 rpm using a Fisher Scientific Marathon 3900 centrifuge, and the supernatant decanted. Additional water was added to the pellet, and the centrifuge/washing steps repeated 3 times to remove excess SUVs and salt/buffer. The pellet was dried overnight in a vacuum oven at RT to quantify the amount of lipid adsorbed on the surface of the silica nanoparticles. For cryo-TEM measurements, the samples were prepared in a slight excess of lipid in order to obtain stable colloidal solutions.

Analysis

Thermogravimetric analysis (TGA). TGA data were obtained on a TA Instruments Hi-Res TGA 2950 Thermogravimetric Analyzer using a ramp rate of 10 °C min^{-1} under a N$_2$ atmosphere. The samples were run from 25 to 800 °C. Derivative plots of the TGA data (DTGA) show regions of maximum rate of weight loss as inflection points, and highlight details of the weight loss as separate thermal events.

FTIR spectroscopy. The SiO$_2$ particles were characterized using Fourier transform infrared spectroscopy (FTIR) in the transmission mode, with 256 scans and a resolution of 2 cm^{-1} using a Mattson Research Series 1 spectrometer (Mattson Instruments, Madison, WI) equipped with a MCT detector.

DLS and ζ-potentials. Dynamic light scattering (DLS) and ζ-potential measurements were obtained on a Malvern Zetasizer Nano-ZS (Malvern Instrument Ltd. Malvern, UK) at 25 °C, with an electric field strength of 30 V cm^{-1} for the ζ-potentials. The natural (unbuffered) pH of the aqueous samples was used. The Smoluchowski equation was used to convert electrophoretic mobilities to ζ-potentials.

Nano-differential scanning calorimetry (Nano-DSC). Nano-differential scanning calorimetry (nano-DSC) measurements were obtained on a TA Instruments (New Castle, DE) Nano DSC-6300. Samples prepared using different ratios of SA$_{SUV}$/SA$_{SiO_2}$ (which had been incubated at 50 °C for 2 h and then stored in the refrigerator) were placed in the nano-DSC at RT, cooled to 5 °C and heated/cooled from 5 to 35 °C at 1 °C min^{-1}. For the time-dependent runs, suspensions with SA$_{SUV}$/SA$_{SiO_2}$ = 1.5, that is with a 1.5 excess of SUVs, were used. The nanoparticle (4 mg ml^{-1}) and SUV (2 mg ml^{-1}) suspensions were prepared separately, mixed at RT and immediately placed in the nano-DSC, which was at 27–28 °C. They were ramped (~1 min) to 30 °C (to slow the kinetics), incubated at various times and then the cooling cycles were measured at 1 °C min^{-1} from 30 °C to 10 °C, to obtain snapshots of the fusion process to form SLBs. The sample was then re-ramped to 30 °C (time approximately 2–3 minutes) and re-cooled to 10 °C. The same procedure was repeated for times up to *ca.* 11 h to 3 days. The samples were in suspension during the nano-DSC runs due to the presence of the excess SUVs.[7]

BET measurements. BET measurements were made on a model ASAP 2020 Micromeritics (Norcross, GA) Surface Area and Porosity Analyzer. Samples were ramped at 10 °C min^{-1} to 150 °C or 180 °C and held at those temperatures for 13–14 h and analyzed by both single point and 5 point methods.

Cryogenic transmission electron microscopy (Cryo-TEM). The supported lipid bilayer suspensions were prepared for cryo-TEM at 25 °C using a Vitrobot (FEI Company), which is a PC-controlled robot for sample vitrification. Quantifoil grids were used with 2 μm carbon holes on 200 square mesh copper grids (Electron Microscopy Sciences, Hatfield, PA). The grid was immersed in the sample, blotted to reduce film thickness, and vitrified in liquid ethane. The sample was then transferred to liquid nitrogen for storage. Imaging was performed using a cooled stage JEOL JEM-2100F TEM (Model 915, Gatan Inc., Pleasanton, CA) at 200 kV.

Results

Characterization of nanoparticles

The results of the nanoparticle characterization by DLS, ζ-potential (ζ), BET measurements, TGA and TEM analysis are presented in Table 1, and representative cryo-TEM micrographs of the 600 °C particles are shown in Fig. 1a. The nanoparticles from Lancaster are not monodisperse even before heat-treatment. There was a combination of single particles with diameters of about 125 nm, as well as "doubles", particles that appeared to have fused during the manufacturing process, with dimensions of

Table 1 Dynamic light scattering, ζ-potential, TEM and TGA weight loss data for SiO$_2$ and SLBs

| Particle type | BET^a | Diameters of SiO$_2$ nanoparticles, [nm] | | | | | | SiO$_2$ Nanoparticles | | SiO$_2$ + SLBs | |
| | | DLS^b | | | | | | | | | |
		z Av. (±10)	PDI^c	Median (±5)	Number Av. (±5)	SA^d Av. (±5)	TEM	ζ-Potential [mV]	TGA % wt loss	TGA % wt loss	Calc.^{e} % wt loss
"as is"		168	0.12	137	108	125	125 ± 5 125 × 200	−45.5 ± 5.5	7.1	5.9	8.3
"as is"+ Pr^f		162	0.12					−38.0 ± 6.8	5.0	6.3	8.3
600 °C	105	173	0.14	140	100	125		−40.2 ± 7.5	0.06	8.2	8.3
600 °C + Pr^f	90	163	0.11	130	105	120	105 ± 10 105 × 160	−43.00 ± 9.70	0.84	8.1	8.3
1000 °C	160	192	0.05	178	162	173		−44.05 ± 6.42	0.009	3.7	5.8
1000 °C + Pr^f	170	198	0.03	195	190	193	120 ± 5 110 × 190	−45.63 ± 6.4	0.040	4.3	5.8
100 nm Nissan SUVs		116 60	0.02			110		−45.2 ± 11.0 0 ± 0.5	1.5	7.2	7.6

^{a} BET surface area converted into spherical particles with diameter D. ^{b} DLS = dynamic light scattering. ^{c} PDI = polydispersity index. ^{d} SA = surface area, after 2 h incubation. ^{e} Based on 125 nm diameter "as-is" and 600 °C SiO$_2$, 185 nm diameter 1000 °C SiO$_2$, with densities of 2.0 g cm^{-3}; and 110 nm diameter Nissan SiO$_2$ with densities of 2.4 g cm^{-3}. ^{f} Pr = piranha.
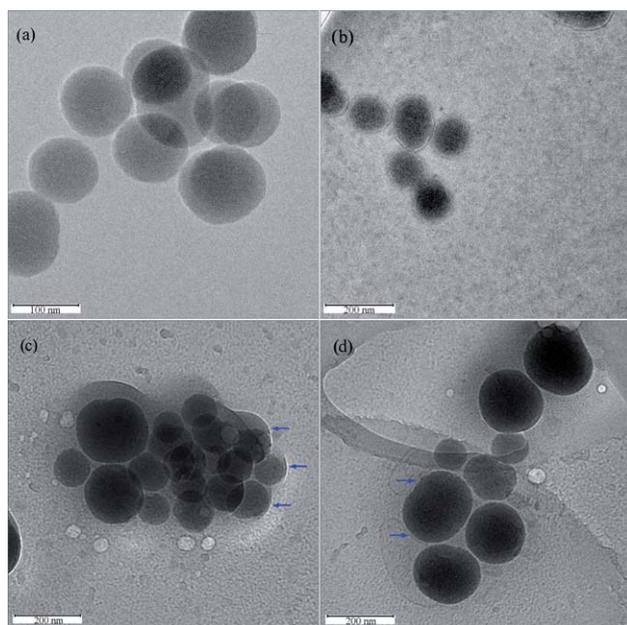

Fig. 1 Cryo-TEM images of: (a) SiO$_2$ heat treated to 600 °C + piranha, and (b) with added DMPC after incubation at 50 °C for 2 h; (c and d) 1000 °C + piranha SiO$_2$ with added DMPC incubated at 50 °C for 2 h. Arrows indicate (c) lipid sheaths and (d) vesicles.

about 125 × 200 nm, and occasionally "triples". This was also observed for the "as-is" SiO$_2$ and SiO$_2$ heat-treated to 1000 °C, with a greater proportion of "doubles" for the 1000 °C SiO$_2$. Not all of the 1000 °C or 1000 °C + piranha SiO$_2$ could be redispersed in water. TGA data indicated that approximately 50% of the original heat-treated sample could be redispersed, and TEM, DLS and ζ-potential data were obtained only for the dispersed fraction. The water content of the "as-is", "as-is" + piranha, and Nissan SiO$_2$ precluded accurate BET measurements due to

adsorbed water (which desorbed and affected pressure measurements), so only BET measurements for the 600 °C, 600 °C + piranha, 1000 °C and piranha + 1000 °C SiO$_2$, which had little, or effectively no adsorbed water (*vida infra*), are reported. Even BET data for the 600 °C + piranha give dimensions that are too small for the same reason. DLS data are reported as the z-average, which assumes single exponential decay of the correlation function and preferentially weights larger size particles. The DLS data were also analyzed and reported by number and surface area averages. The closeness in size between the "singles" and "doubles" makes it difficult to separate them by DLS. The Nissan nanobeads are more uniform, and smaller in size, *ca.* 110 nm in diameter by DLS, with no "dimers". When calculating SA$_{SUV}$/SA$_{SiO_2}$ ratios, diameters based on DLS surface areas were used, since surface area is the parameter required for the amount of lipid needed for coverage of the SiO$_2$. Values of 125 nm for the "as-is" and 600 °C SiO$_2$, 185 nm for the 1000 °C SiO$_2$ and 105 nm for the monodisperse Nissan SiO$_2$ were used in the calculations. ζ-Potential data for the nanoparticles indicate that all the Lancaster beads, whatever the heat/piranha treatment, as well as the Nissan beads, had similar ζ-potentials of around −45 ± 5 mV. The solutions were diluted until constant values of the ζ-potentials were obtained.

Fig. 2 shows the FTIR spectra of the "as-is", "as-is" + piranha, 600 °C, 600 °C + piranha, 1000 °C, 1000 °C + piranha, and Nissan SiO$_2$. The nanoparticles were vacuum dried overnight and then heated for *ca.* 4 h at 150 °C before the IR spectra were measured. The bands observed are the isolated silanol vibrations at 3740 cm^{-1}, the hydrogen-bonded silanols at 3600 cm^{-1}, and bands associated with adsorbed water (3400–3500 cm^{-1}).[36] For the "as-is" SiO$_2$, made from condensation of TEOS, residual bands associated with the methyl and methylene vibrations of (CH$_2$CH$_2$O)– can be observed.[37] Acid treatment removes these bands, suggesting that they were mainly on the surface of the nanoparticles. Heat treatment at 600 °C and 1000 °C also results in removal of the hydrocarbons. In addition, as the heat
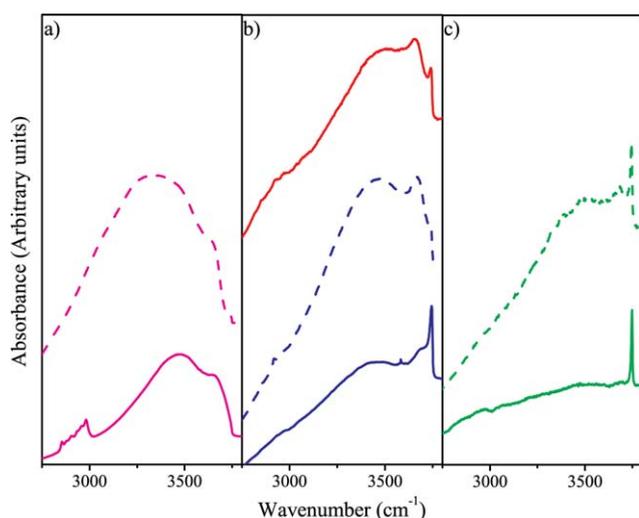
Fig. 2 FTIR spectra between 2750 and 4000 cm^{-1} of nominal 100 nm SiO$_2$ nanoparticles with different thermal/chemical treatments: (a) "as-is" (solid line), "as-is" + piranha (dashed line); (b) 600 °C" (blue solid line), 600 °C + piranha (dashed line); Nissan SiO$_2$ (red solid line), and (c) 1000 °C (solid line), 1000 + piranha (dashed line).

treatment temperature increases, the silanol density decreases, the ratio of the isolated/H-bonded SiOH increases, and the amount of adsorbed water decreases. Subsequent acid treatment of the heat-treated samples recovers some of the H-bonded silanols, but never to levels comparable to the "as-is" SiO$_2$. The "as-is" SiO$_2$ from Nissan, made by a water–glass process, has no organic component, and has FTIR spectra most comparable to the 600 °C + piranha treated SiO$_2$.

The trends observed in the FTIR data are confirmed by TGA analysis of the SiO$_2$, shown in Fig. 3 and summarized in Table 1. The inset in Fig. 3 shows derivative (DTGA) weight loss data for the SiO$_2$. Weight losses are greatest for the "as-is" nanobeads, and decrease to minimal amounts for the nanobeads heat-treated at 1000 °C. The weight loss due to physically adsorbed water,
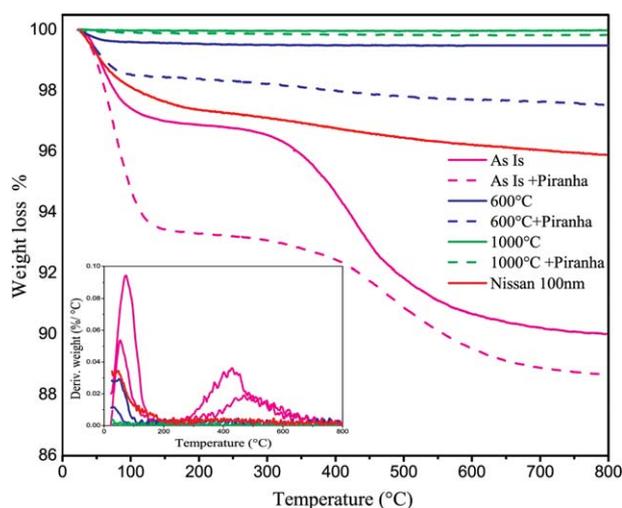
which occurs below *ca.* 100 °C, is greatest for the "as-is" nanobeads and least for the nanobeads heat-treated at 1000 °C. Piranha treatment increases the surface silanol density and thus weight loss, at each heat-treatment temperature, as well as the amount of physically adsorbed water. The former statement is true except for the "as-is" SiO$_2$ compared with the "as-is" + piranha SiO$_2$ and is due to the replacement of the higher mass hydrophobic groups with SiOH.

Characterization of SUVs and supported lipid bilayers

The SUVs had *z*-average diameters of 60 nm ± 5 nm and ζ-potentials of 0 ± 0.5 mV (Table 1). TGA weight loss data for the lipids + nanoparticles (incubated for 2 h at 50 °C) are presented in Table 1, and compared with calculated values based on 125 nm ("as-is" and 600 °C), 185 nm (1000 °C) and 110 nm (Nissan) diameters. Both the 600 °C and Nissan SiO$_2$ have the expected weight losses, but the 1000 °C has 64–74% less and the "as-is" sample has 70–75% less, than the calculated values, respectively. Derivative TGA data for the nanobeads with adsorbed lipids are shown in Fig. 4, where the peaks originating from water loss clearly show the order "as-is" + piranha > "as-is" > 600 °C + piranha > 600 °C > (1000 °C + piranha ≈ 1000 °C) ≈ 0, the same order as for the pure nanoparticles. The peaks at 240–270 °C and 300 °C in the DTGA traces, attributed to lipid decomposition of the head-group and hydrocarbon tail, respectively,[38] are similar in appearance for the 600 °C, 600 °C + piranha, 1000 °C and 1000 °C + piranha. The lipid peaks on the Nissan nanoparticles are also narrow, but shifted down in temperature. For the "as-is" and "as-is" + piranha, the peaks are broader and occur at higher temperature; this cannot be attributed to the underlying SiO$_2$ since the derivative weight loss peaks (inset, Fig. 3) show no features in this temperature region. It is possible that some of the chains, once water is removed, can adsorb to the silica surface, spreading out the range of decomposition temperatures.

Fig. 3 TGA and DTGA (inset) weight loss of heat and piranha treated nominal 100 nm SiO$_2$, and nominal 100 nm Nissan SiO$_2$, nanobeads.
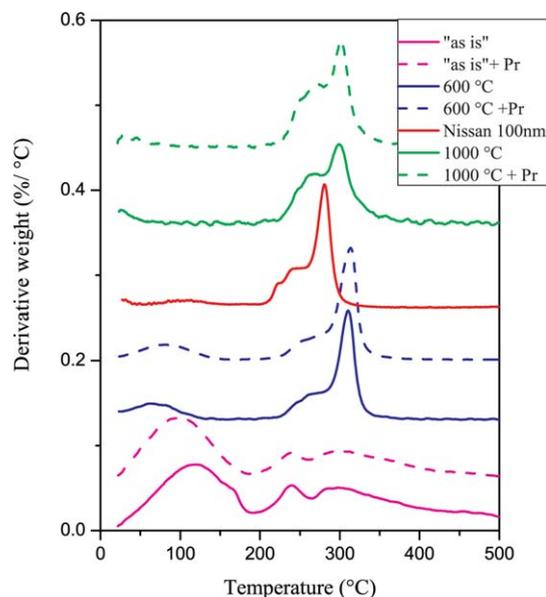

Fig. 4 DTGA weight loss data of adsorbed DMPC lipid bilayers on nominal 100 nm SiO$_2$ nanoparticles with different thermal/chemical treatments; Pr = piranha.

Table 2 Phase transition temperatures and enthalpies for DMPC MLVs, SUVs and SLBs

SUVs, MLVs and SLBs		$T_m/^{\circ}C$	ΔH_m/kcal mol^{-1}	$T_c/^{\circ}C$	ΔH_c/kcal mol^{-1}
MLVs		24.0	5.43	23.8	5.41
SUVs		24.2	5.26	24.4	5.27
SLBs					
	Nissan	22.5	3.20	22.1	3.24
	As is + piranha	21.7	2.57	21.0	2.75
	600 °C + piranha	21.9	2.75	21.4	2.77
	1000 + °C + piranha	21.6	4.89	20.4	3.39
			$\langle 3.35 \rangle$		$\langle 3.03 \rangle$
			3.35/5.26 = 63.6%		3.03/5.27 = 57%

In order to investigate the effect of surface water on lipid fusion to form SLBs, nano-DSC traces were obtained as a function of SA_{DMPC}/SA_{SiO_2} for the "as-is" + piranha, 600 °C + piranha, 1000 °C + piranha, and the Nissan "as-is" SiO$_2$. The piranha treated SiO$_2$ were used, since they provided a range of surface properties, the piranha treatment was likely to hydrolyze interparticle silanol condensation of the nanoparticles after heat treatment, and remove ethoxy groups. The gel-to-liquid phase transition temperatures of DMPC on supported lipid bilayers have been previously identified.[6] These transitions on heating (T_m) and cooling (T_c), and their respective enthalpies, ΔH_m and ΔH_c, are presented in Table 2. For comparison, the same thermodynamic data are presented for DMPC MLVs and SUVs. The melt and crystallization temperatures of the SUVs are very slightly higher than those of the MLVs, as we have previously observed.[7] The SLBs have T_ms decreased by 1.7–2.6 °C and T_cs decreased by 2.3–4 °C compared with the MLVs and SUVs. In general, $T_c \approx T_m$ for the MLVs and SUVs, but $T_m > T_c$ for the SLBs; this occurs since equilibrium is reached more quickly for lipids in MLVs and SUVs than lipids on the solid supports.[6] Although the effect is small, T_m, T_c (Nissan) > T_m, T_c (600 °C + piranha) > T_m, T_c ("as-is" + piranha) > T_m, T_c (1000 °C + piranha). The average values of the transition enthalpies, ΔH_m

and ΔH_c, are smaller for the SLBs than for the SUVs by 64% and 57% respectively.

Fig. 5 shows nano-DSC traces for the 600 °C + piranha SiO$_2$ incubated for 2 h at 50 °C as a function of SA_{DMPC}/SA_{SiO_2} for the 2nd cooling cycle. Below SA_{DMPC}/SA_{SiO_2} = 1, only a single transition is observed, which originates from the gel-to-liquid transition of DMPC on supported lipid bilayers (SLBs).[4,6] For SA_{DMPC}/SA_{SiO_2} > 1, the peak due to T_c from DMPC SUVs is observed, which increases with increasing amount of DMPC in the suspension. The peak height or area ratio of the SLB peak, I_{SLB}, to that of the total, $I_{SLB}/(I_{SLB} + I_{SUV})$ is proportional to the amount of excess SUVs that are in the suspension. However, the enthalpy of the transition for SLBs is 64–57% of that for SUVs. Therefore,

$$I_{SLB}/I_{Tot} = \Delta H_{SLB}\,(\#SLBs)/[\Delta H_{SLB}\,(\#SLBs) + \Delta H_{SUV}\,(\#SUVs)]$$
$$= 0.6\,(\#SLBs)/[0.6(\#SLBs) + (\#SUVs)],$$

if an average of $\Delta H_{SLB} = 0.6\Delta H_{SUV}$ is used. For example, if SA_{SUV}/SA_{SiO_2} = 1.5, there would be 1 SLB and 0.5 SUV, so that I_{SLB}/I_{Tot} = 0.56. This is approximately what is observed for the SA_{SUV}/SA_{SiO_2} = 1.5 sample. However, these results are only qualitatively correct for several reasons. In addition to the errors inherent in determining the sizes of the nanoparticles, the SA_{SUV}/SA_{SiO_2} ratio was calculated based on planar surfaces. In fact, the particles due to their curvature can accommodate more than the calculated amount of lipid.[6]

A plot of #SUVs/#SLBs for the "as-is" + piranha, 600 °C + piranha, 1000 °C + piranha, and Nissan beads obtained after a 2 h incubation at 50 °C is shown in Fig. 6. The intensities were corrected in order to obtain the ratio for the number of SUVs to the number of SLBs (#SUVs/#SLBs). We had first expected that the SiO$_2$ with the highest SiOH density would have the greatest adsorption of DMPC, and the SiO$_2$ with the lowest SiOH density would have the least DMPC adsorption at comparable #SUVs/#SLBs ratios. The SiO$_2$ heated to 1000 °C with very few silanols did have the least SLB formation. However, the SiO$_2$ heated at 600 °C + piranha had greater adsorbed DMPC than the "as-is" + piranha for the same ratio of #SUVs/#SLBs.

Time dependent adsorption experiments confirmed this trend. Fig. 7 presents nano-DSC plots on cooling of the "as-is" + piranha, 600 °C + piranha, 1000 °C + piranha, with SA_{SUV}/SA_{SiO_2} = 1.5 as a function of time. Since excess SUVs were always present, the transition attributed to T_c (SUVs) never disappeared. At fixed SA_{SUV}/SA_{SiO_2}, the intensity ratio of SUVs/SLBs was greatest for the 1000 °C + piranha SiO$_2$, and was

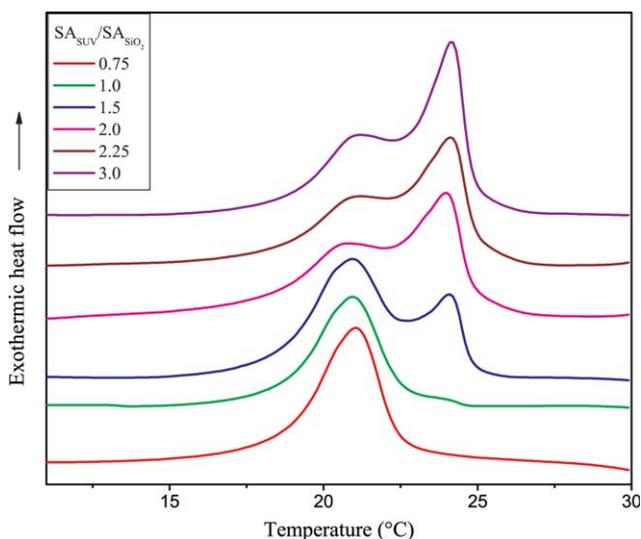**Fig. 5** Nano-DSC traces for nominal 100 nm, 600 °C + piranha SiO$_2$ as a function of SA_{DMPC}/SA_{SiO_2}.
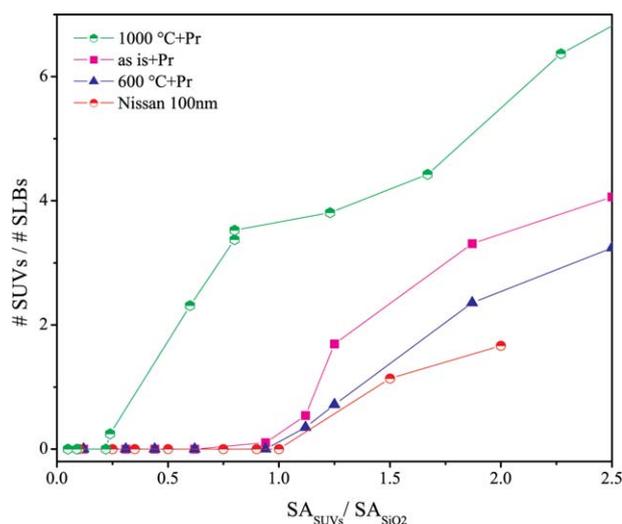
Fig. 6 #SUVs/#SLBs as a function of time for nominal 100 nm SiO_2 with different thermal/chemical treatments: "as-is"+ piranha, 600 °C + piranha, 1000 °C + piranha, and Nissan 100 nm SiO_2. Nano-DSC data obtained after incubation of SiO_2 with DMPC SUVs for 2 h at 50 °C. Measurement of peak height ratios of SUVs and SLBs converted to #SUVs/#SLBs by normalization using their respective enthalpies, ΔH_m (SUVs) and ΔH_m (SLBs).
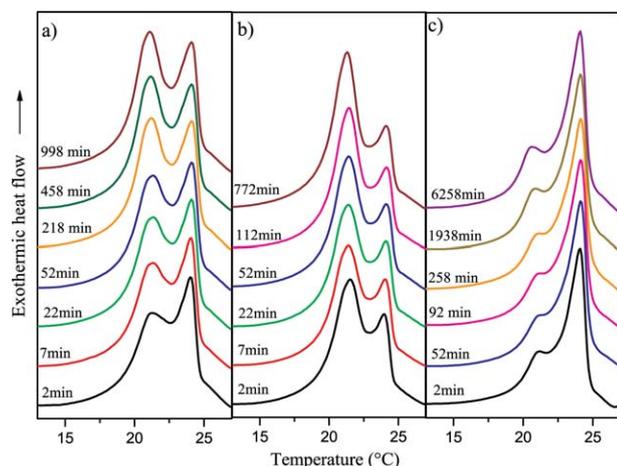

Fig. 7 Nano-DSC traces of SLB formation when $SA_{DMPC}/SA_{SiO_2} = 1.5$ as a function of time for nominal 50 nm DMPC SUVs incubated at 30 °C with nominal 100 nm SiO_2 and the following thermal/chemical treatments: (a) as is + piranha; (b) 600 °C + piranha; (c) 1000 °C + piranha.

greater for the "as-is" + piranha than for the 600 °C + piranha at comparable times. The peak attributed to SUVs was always larger than the SLB peak for the 1000 °C + piranha SiO_2. The reverse was true for the 600 °C + piranha SiO_2: the SLB peak was always greater than the SUV peak. By contrast, the greatest change occurred for the "as is" + piranha SiO_2, where the SUV peak was initially larger, and was finally slightly lower than the SLB transition. Since as discussed above for the $SA_{SUV}/SA_{SiO_2} =$ 1.5, the ratio of intensities, I_{SLB}/I_{Tot}, for the 600 °C + piranha is approximately what is expected based on the measured ΔH, there is never complete SLB formation for either the 1000 °C + piranha or "as is" + piranha SiO_2, in agreement with the TGA results.

There are other interesting observations that can be made from these data. Much of the SLB formation occurs at relatively short times for both 600 °C + piranha and 1000 °C + piranha SiO_2. SLB formation on the 1000 °C + piranha SiO_2 was small, and changed little with time for periods up to 4 days. Similarly, much of the SLB formation had occurred after 2 minutes for the 600 °C + piranha SiO_2. However, for the as is + piranha SiO_2, although there was significant SLB formation after 2 minutes, more SLB did occur for another 3–4 hours, and then remained constant. This clearly indicates that some SLB formation occurs very quickly for all the SiO_2, but that the rate of SLB formation becomes slower for the as is + piranha SiO_2 compared with the 600 °C + piranha SiO_2.

Cryo-TEM data for the 600 °C + piranha SiO_2 are presented in Fig. 1b and show SLB formation around the nanoparticles with no SUVs present. The 1000 °C + piranha sample (Fig. 1c and d) shows what appears to be clusters of nanoparticles surrounded by a lipid membrane sheath, as well as 50–60 nm SUVs, and larger SUVs adsorbed but not fused to the nanoparticles. Comparatively, the 600 °C + piranha shows individual nanoparticles surrounded almost completely by SLBs with little evidence of free SUVs. This comparison is consistent with Fig. 6 and 7, which show greater SLB formation and fewer free SUVs for 600 °C + piranha than for 1000 °C + piranha.

Discussion

The effect of surface water on nominal 100 nm SiO_2 nanoparticles, which had been heated to various temperatures and treated with piranha solution, on the adhesion/fusion of SUVs of zwitterionic DMPC, was investigated. Thermal/chemical treatments affected the silanol densities and thus the amount of bound water to the silica surface. Although we expected that both the amount and rate of SUV fusion to form SLBs would increase with increasing silanol density, it was found instead that the surface with a lower silanol density (600 °C + piranha) had a higher rate of vesicle fusion compared with the surface with higher ("as-is" + piranha) silanol density, and had higher coverage, as monitored by TGA, after a 2 h incubation, as well as by time dependent nano-DSC thermograms. If only the number of "contact points," in this case charged silanol groups, between the SUVs and surface determined vesicle rupture[3] the order would be reversed. This suggests that the organization of water next to a solid surface plays an important role in lipid fusion onto the surface. The water around the lipid headgroup is expected to be the same in all cases.

In order to understand the effects of water, it is useful to review the interactions that exist between SUVs–SUVs, SiO_2–SiO_2 and SUVs–SiO_2. Zwitterionic SUVs interact with each other through weak van der Waals (attractive) and thermal undulation/protrusion (repulsive) forces. The dominant interaction between negatively charged SiO_2 is electrostatic in origin, but hydrophobic attraction of Si–O–Si groups can occur on highly dehydroxylated surfaces. In the case of SUV–SiO_2 interactions, the attractive van der Waals and thermal undulation/protrusion repulsive forces would be expected to be similar, but electrical double layer and hydration forces might be expected to be different as the SiO_2 surface properties changed.

The fusion of zwitterionic lipids to form supported lipid bilayers may thus be affected by both electrical double layer and hydration forces. In fact, the major driving force for adhesion between SUVs and silica was suggested to be the electrostatic attraction between the two surfaces, which for zwitterionic lipids (with zero potential) was proportional to the square of the ζ-potential, ζ, or charge density, σ, of the silica.[2] Although the isoelectric point of zwitterionic egg phosphatidylcholine (PC), pI = 4.13,[39] might suggest that the DMPC would have a slightly negative charge at pH = 8, and thus be repelled by the negatively charged SiO_2 surface, the measured ζ potentials of the DMPC SUVs investigated here were zero within experimental error, and thus should not affect the electrostatic interaction. More importantly, we do not see much difference between ζ of the "as-is" or heat treated silicas, with or without piranha treatment, which were all ca. -45 ± 5 mV. The same ζ-potentials were measured although the total silanol densities were very different, as determined both by FTIR and TGA data. Similarity in ζs could occur if only the isolated SiOHs contributed to the ζ-potential, which would happen if only the isolated SiOH, and not the hydrogen-bonded silanols, dissociated to give a negatively charged surface.

Evidence that this is the case comes from second harmonic generation (SHG) data. Silanol densities on fully hydroxylated silica surfaces are reported to be about 4.9 SiOH per nm^2,[36,40] composed of isolated silanols and hydrogen-bonded silanols, where the latter can be directly hydrogen bonded with each other (46%), or through a bridging water molecule (35%).[1] The surface populations of the isolated and hydrogen bonded SiOH inferred from SHG data were estimated to be 19% and 81%, respectively, with pK_a values of 4.9 and 8.5,[1] consistent with the view that isolated silanols can more readily dissociate compared with the hydrogen-bonded silanols.[36] In the current investigation, at the pH = 7, where the ζ-potentials of the SiO_2 in pure water were obtained or at pH = 8.0, where the fusion experiments were performed, only the isolated silanols would be expected to dissociate on any of the SiO_2 surfaces, resulting in similar charge densities. In addition, for the buffered solutions at pH = 8, there is charge shielding of the nanoparticles. The surface charge density at this pH has been reported as 0.2C m^{-2}.[1,36]

Since surface charge density differences, and thus electrostatic interactions between the neutral SUVs and similarly charged SiO_2 surfaces, are therefore not expected to play a major role in the differences between the adsorption/fusion processes, what is left is only hydration repulsion between the SUVs and SiO_2 or hydrophobic attraction between the SiO_2. The former interaction is critical to explain the difference between the "as-is" SiO_2 and the SiO_2 heat treated to 600 °C. For the SiO_2 heat treated to 1000 °C, which will be discussed first, there were few silanols and little adsorbed water, so that hydrophobic interactions between the nanoparticles are important.

At very low silanol densities, when there were mainly isolated surface silanols as shown by FTIR and TGA data, it was difficult to form supported lipid bilayers. TGA data indicated that less than the expected lipid coverage was found on the nanoparticles. Cryo-TEM data showed that the SiO_2 formed aggregates in suspension, surrounded by a supported lipid bilayer sheath. SUVs could be observed adsorbed to, but not forming a SLB on some of the nanoparticles. At these low SiOH densities for SiO_2 heat

treated at 1000 °C, the silica has many hydrophobic surface Si–O–Si groups. In fact, only approximately 50% of the 1000 °C SiO_2 could be resuspended, indicating that the remainder was so hydrophobic that it could not be wet by water. The SiO_2 that could be resuspended was found to form clusters due to hydrophobic interactions between the nanoparticles, with some silanols on the exterior of the clusters promoting SLB formation around the whole cluster. On fully hydrated planar silica surfaces, it has been shown that isolated silanols separated by >120 Å^2 were about 12% of the isolated silanols.[41] After heat treatment, this number should increase leaving large hydrophobic areas that can associate. It has also been suggested, and may be the case here, that for silica heated above 650 °C, the adsorption/fusion of DMPC does not occur through a water-mediated interaction. Instead, there is direct adsorption of DMPC headgroups to defect sites, which have been observed as pits on a planar SLB silica surface that disrupted lateral assembly of the bilayer.[42]

The increased attraction between the SUVs and 600 °C SiO_2 compared with the "as-is" SiO_2 can be explained by increase of hydration repulsion in the latter case, due to the differences in adsorbed water on the two SiO_2 surface. Hydration repulsion is a short range force that exists between two approaching hydrophilic surfaces in water, and has been attributed to the energy needed to remove the water of hydration between interacting surfaces that contain ionic or polar species.[43,24] Water near a silica surface is known to be different than that of bulk water, and this interfacial water layer, which has been extensively investigated at both the solid/air and solid/liquid interface,[44] can be affected by the properties of the underlying silica surface,[45,46] in particular by the type, number and distribution of silanol groups. Using ab initio calculations of cluster models of SiO_2, with one or two (neighboring) SiOH on the surface as surrogates for isolated and hydrogen bonded silanols, a stable water layer was found with two SiOH, which disappeared when there was only one SiOH, although water molecules were still found around the isolated SiOH.[42]

Optical SFG has been extremely useful in characterizing the adsorbed water layer on SiO_2. Both disordered and quasi-ice like or ice-like properties of water have been observed near amorphous silica[45] and crystalline quartz surfaces.[46] Fused quartz or silica, with a pK_a of 3, can have varying degrees of ionization, depending on the pH.[36] When the silanols of quartz are neutral (undissociated, pH < 2–3) or fully ionized (all dissociated, pH > 10), the structure of water at the surface is ice-like, as determined by optical SFG, with fewer ordered H_2O layers (1–2) when the weaker hydrogen bonding compared with the stronger electrostatic field force (3–5 ordered water layers) provides the ordering of the interfacial water layer.[47] Since the orientation of water at the surface was found to be opposite for the two extreme cases, with the dipoles of water oriented into the solid (oxygens pointing away from the surface) at high pH, and with the oxygens oriented towards the surface at low pH, at intermediate pHs, disordering of the water occurred as a function of the degree of ionization, due to the competing alignment effects.[47] The more disordered water had a maximum at pH = 8,[48] so that at pH = 8 of the current experiments, the effects of the "water-like" H_2O are expected to be most pronounced. We postulate that it is this disordered layer that must be removed before fusion of the DMPC SUVs to the SiO_2 surface can occur, and that there is
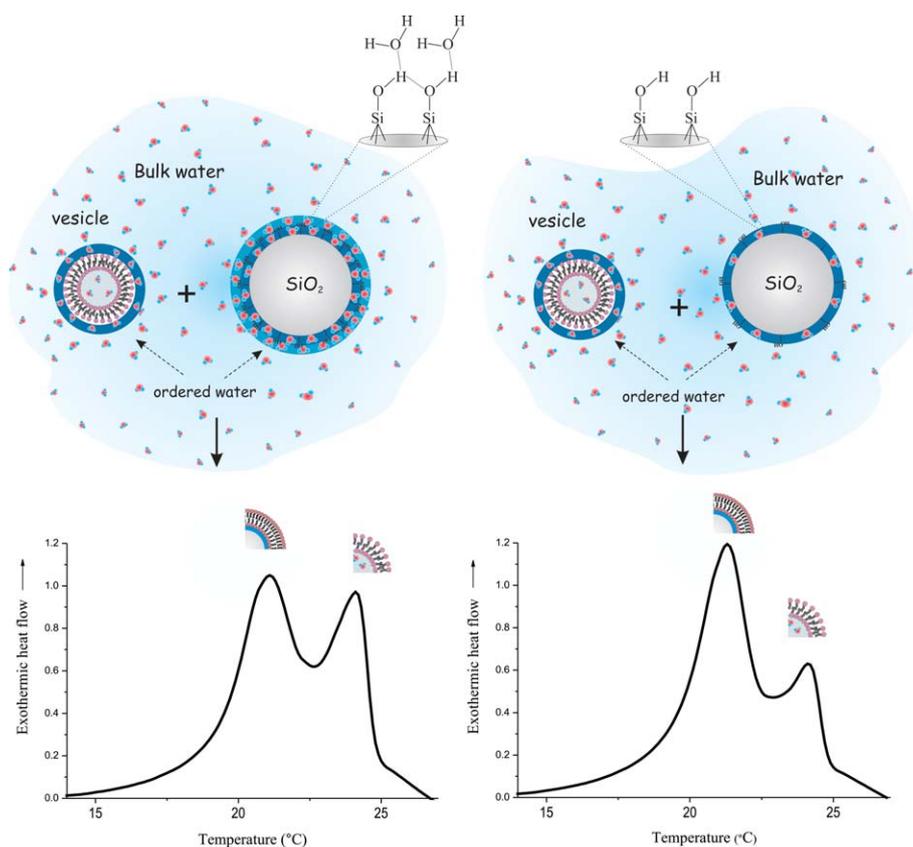
Fig. 8 Schematic of SLB formation of nominal 50 nm DMPC SUVs onto nominal 100 nm SiO_2 nanoparticles with different thermal/chemical treatments. The (left) "as-is" + piranha SiO_2 had a higher silanol density and more bound water than the (right) 600 °C + piranha SiO_2. The bound water is shown schematically (not to scale) as more ordered (dark blue) and more disordered (light blue). The increased hydration repulsion as the result of removal of more bound water from the more hydrated SiO_2 results in decreased rate of SLB formation on the more hydrated SiO_2. The ordered water around the SUVs is the same in both cases. After SLB formation, the ordered water is not shown for clarity. The nano-DSC thermograms at comparable times for the two SiO_2 show more SLB formation for the less hydrated SiO_2.

a greater amount of disordered water on the fully hydrated (as-is) than on the partially condensed (600 °C) SiO_2. This is shown schematically in Fig. 8.

Thus, although the substrate material affects the formation process and character of adsorbed/fused bilayers, the interaction must be mediated by the structure of this water layer, which in turn is affected by the underlying substrate. The decrease in hydrogen-bonded compared with isolated silanols and the corresponding decrease in adsorbed water with increase in heat-treatment temperature are clearly observed for the SiO_2 nanoparticles in the current investigation by both TGA and FTIR spectroscopy. This effect has also been observed for Stöber SiO_2 (8 and 260 nm) nanoparticles, where the ratio of hydrogen bonded to isolated silanols decreased with decreasing particle size, and where the amount of hydrogen bonded water to the silicas (as measured using NIR spectroscopy) also decreased.[49] This effect was explained by polarization differences between silanols: hydrogen bonding between SiOH on the silica resulted in polarization in other SiOH, promoting hydrogen-bonding with water molecules. Since polarization of isolated silanol groups was less than for hydrogen-bonded SiOH, there was less hydrogen bonded water.[49]

The increased hydration repulsion between the SUVs and the "as-is" compared with the 600 °C SiO_2 can thus be explained by

a model in which both contain a more tightly bound "ice-like" water layer, with a more disordered water layer that is greater for the "as-is" SiO_2. When the SUVs approach the SiO_2 surface, more energy must be expended to remove this greater amount of water from the "as-is" SiO_2. Although it might be expected that the entropy gain would be greater for the more hydrated silica surfaces, and thus the interaction should be more favorable for these surfaces, we observed the opposite. Therefore, this entropy gain is not sufficient to offset the unfavorable hydration repulsion for the more hydrated surfaces.

The water from the DMPC headgroups must also be removed. However, removal of this water would be the same in all cases considered here. Further, it has been shown by dynamic AFM measurements that the water surrounding lipid bilayers is more disordered in the liquid crystalline compared with the gel phase, and requires lower force for removal.[29] This may partially explain why SLB formation is typically accomplished (as has been done in this investigation) by incubating the DMPC with the SiO_2 nanoparticles above the T_m of the lipids.

The proposed model is consistent with SHG data of neutral lipid egg phosphatidylcholine (egg PC) on SiO_2 at all pH values, which showed that the strength of the ice-like mode was very similar to the bare quartz surface, but the water-like mode oscillator strength was suppressed.[48] The data were interpreted as

resulting from PC replacement of the liquid-like interfacial water, leaving the 1–2 layers of ice-like water.[50,51] The current results are also in agreement with a study of DMPC adsorption onto planar hydrophilic SiO_2 surfaces in which the silanol density was reduced by temperature induced dehydroxylation. In this case, water contact angles were between <5° (as prepared) and 67° (700 °C per 1 h), where 90° is regarded as the boundary between "hydrophilic" and "hydrophobic" surfaces. The SLBs had a higher affinity for the less hydrophilic surface and the formation of SLBs of DMPC was accelerated as the SiOH density decreased.[42,52]

Hydration repulsion has been shown to be important in vesicle–vesicle and vesicle–surface interactions. The hydration shells in zwitterionic lipid MLVs, where water layers alternate between the bilayers, were estimated to occupy a layer about 0.5 nm thick around the polar headgroups, leaving a layer of $ca.$ 1.7 nm of "free water" in the center of the inter-bilayer space free.[24] The overall structure was shown to be determined by a balance between long-range attractive forces, van der Waals interactions between the lamellae, and repulsive hydration forces,[25] which decayed exponentially with a decay distance of $ca.$ 0.2 nm.[24] Hydration repulsion was also used to account for the decrease in aggregation of Stöber SiO_2 (8 and 260 nm) with increasing particle size, where there was an increase in the hydrogen-bonded water layer for the larger particles that increased the repulsive hydration force between them.[49]

A similar effect, in which ions instead of water needed to be removed from the space between SUVs and a surface, has been invoked to explain the absence of SLB formation of zwitterionic lipids onto charged surfaces when the large molecular ion of the buffer was of opposite charge to that of the surface. In this case, there was high entropic or osmotic repulsion (electric double layer repulsion) as the two surfaces approached each other, since the counterions had to be squeezed into a smaller and smaller space, which was more difficult the larger the counterion.[3]

Although the current investigation has pointed out the effects of the water layer on SiO_2 substrates on the formation of SLBs, most silica used to form SLBs has sufficient adsorbed water that SLB formation occurs readily, although the formation times may be different depending on the type of SiO_2 used. The water structure on other substrate materials may play a similar role. Lastly, there are slight differences in transition temperatures between the Nissan (made by a water–glass process) and Lancaster (made by a Stöber process) SiO_2. The higher T_m and T_c of the Nissan nanoparticles by 0.6 to 0.9 °C and 0.7 to 1.7, respectively, suggest better lipid packing for the Nissan nanoparticles, but we are not sure of the reason. The FTIR spectra of the Nissan SiO_2 and the Lancaster 600 °C + piranha treated SiO_2 are close in appearance, and these two samples in fact behave most similarly (e.g. their calculated and observed lipid TGA weight losses are equal, the T_m and T_c values and the amount of adsorbed water are closest), confirming the importance of the underlying surface and water structure. The slight decrease in T_m and T_c for 600 °C > "as is" > 1000 °C SiO_2 may reflect the decreased amount of lipid on the nanoparticles, which can result in defects at the edges of regions without lipids. The DTGA data suggest that whatever lipid is on the 1000 °C is similar to what was on the other samples, i.e. in SLB form. This was also confirmed by FTIR data for DPPC on the four types of SiO_2, which showed the all-trans symmetric and asymmetric CH_2 stretches at the same wavenumbers, albeit weaker, for DPPC on the 1000 °C SiO_2.[53]

Conclusions

Silica nanoparticles of nominal 100 nm diameter size were characterized by dynamic light scattering, FTIR and ζ-potential measurements. They were heat or heat and piranha treated up to 1000 °C to vary the silanol density. Increasing heat-treatment temperature decreased the total silanol density, increased the relative amount of isolated compared with hydrogen bonded silanols and decreased the amount of adsorbed water. Piranha treatment recovered some but not all the silanols condensed at a particular temperature. ζ-Potential measurements were similar for all the SiO_2, consistent with SHG data from the literature indicating that at pH = 8, ionization occurred only for the isolated silanols. Adsorption/fusion of 60 nm DMPC SUVs onto fully hydrated SiO_2 ("as-is"), and SiO_2 dehydroxylated by heat treatment, was measured after 2 h incubation with the SUVs and as a function of time. The fusion process was measured by monitoring the intensities of the gel-to-liquid crystal phase transition temperatures on the cooling cycle (T_c) for the SUVs and SLBs, which differed in temperature by approximately 2 °C. Since the enthalpy of the transition ΔH (SLB) ≈ $0.6\Delta H$ (SUV), the ratio of the #SUVs/#SLBs was corrected by this amount. SLB formation occurred more slowly on the fully hydroxylated SiO_2 than on SiO_2 heated/piranha treated at 600 °C. Since the two SiO_2 were similar in other respects, in particular their charge (ionization), as determined by ζ-potential measurements, differences in electrostatic interactions between the neutral DMPC and SiO_2 could not account for the difference. Therefore, the increased rate for the less hydroxylated surface was attributed to decreased hydration repulsion. Cryo-TEM data confirmed SLB formation. The decreased amount of SLB formation for the 1000 °C + piranha SiO_2 was attributed to hydrophobic association of the drastically dehydroxylated SiO_2 surfaces that contained Si–O–Si hydrophobic patches. Cryo-TEM images showed SiO_2 aggregates surrounded by lipid sheaths, SUVs and SUVs adsorbed but not fused to the nanoparticles.

Abbreviations

SLBs	supported lipid bilayers
MD	molecular dynamics
SUVs	small unilamellar vesicles
MLVs	multilamellar vesicles
DMPC	1,2-dimyristoyl-sn-glycero-3-phosphocholine
DLS	dynamic light scattering
PBS buffer	$Na_2HPO_4 \cdots 7H_2O$ and $NaH_2PO_4 \cdots H_2O$
nano-DSC	nano-differential scanning calorimetry
TGA	thermogravimetric analysis
DTGA	derivative TGA
SiO_2	silica
Pr	piranha

References

1 S. W. Ong, X. L. Zhao and K. B. Eisenthal, Polarization of water-molecules at a charged interface—2nd harmonic studies of the

silica water interface, *Chem. Phys. Lett.*, 1992, **191**(3–4), 327–335.

2   T. H. Anderson, Y. J. Min, K. L. Weirich, H. B. Zeng, D. Fygenson and J. N. Israelachvili, Formation of supported bilayers on silica substrates, *Langmuir*, 2009, **25**(12), 6997–7005.

3   T. Cha, A. Guo and X. Y. Zhu, Formation of supported phospholipid bilayers on molecular surfaces: role of surface charge density and electrostatic interaction, *Biophys. J.*, 2006, **90**(4), 1270–1274.

4   C. Naumann, T. Brumm and T. M. Bayerl, Phase transition behavior of single phosphatidylcholine bilayers on a solid spherical support studied by DSC, NMR and FT-IR, *Biophys. J.*, 1992, **63**(5), 1314–1319.

5   S. Mornet, O. Lambert, E. Duguet and A. Brisson, The formation of supported lipid bilayers on silica nanoparticles revealed by cryoelectron microscopy, *Nano Lett.*, 2005, **5**(2), 281–285.

6   S. Ahmed and S. L. Wunder, Effect of high surface curvature on the main phase transition of supported phospholipid bilayers on SiO$_2$ nanoparticles, *Langmuir*, 2009, **25**(6), 3682–3691.

7   S. Savarala, S. Ahmed, M. Ilies and S. L. Wunder, Formation and colloidal stability of DMPC supported lipid bilayers on SiO$_2$ nanobeads, *Langmuir*, 2010, **26**(14), 12081–12088.

8   Q. Liang, Q. H. Chen and Y. G. Ma, Membrane-mediated interactions between nanoparticles on a substrate, *J. Phys. Chem. B*, 2010, **114**(16), 5359–5364.

9   E. Sackmann, Supported membranes: scientific and practical applications, *Science*, 1996, **271**(5245), 43–48.

10 B. Seantier, C. Breffa, O. Felix and G. Decher, Dissipation-enhanced quartz crystal microbalance studies on the experimental parameters controlling the formation of supported lipid bilayers, *J. Phys. Chem. B*, 2005, **109**(46), 21755–21765.

11 I. Pfeiffer, B. Seantier, S. Petronis, D. Sutherland, B. Kasemo and M. Zach, Influence of nanotopography on phospholipid bilayer formation on silicon dioxide, *J. Phys. Chem. B*, 2008, **112**(16), 5175–5181.

12 I. Pfeiffer, S. Petronis, I. Koper, B. Kasemo and M. Zach, Vesicle adsorption and phospholipid bilayer formation on topographically and chemically nanostructured surfaces, *J. Phys. Chem. B*, 2010, **114**(13), 4623–4631.

13 C. A. Keller and B. Kasemo, Surface specific kinetics of lipid vesicle adsorption measured with a quartz crystal microbalance, *Biophys. J.*, 1998, **75**(3), 1397–1402.

14 E. Reimhult, F. Hoeoek and B. Kasemo, Intact vesicle adsorption and supported biomembrane formation from vesicles in solution: influence of surface chemistry, vesicle size, temperature, and osmotic pressure, *Langmuir*, 2003, **19**(5), 1681–1691.

15 R. P. Richter and A. Brisson, QCM-D on mica for parallel QCM-D-AFM studies, *Langmuir*, 2004, **20**(11), 4609–4613.

16 R. P. Richter and A. R. Brisson, Following the formation of supported lipid bilayers on mica: a study combining AFM, QCM-D, and ellipsometry, *Biophys. J.*, 2005, **88**(5), 3422–3433.

17 T. E. Starr and N. L. Thompson, Formation and characterization of planar phospholipid bilayers supported on TiO$_2$ and SrTiO$_3$ single crystals, *Langmuir*, 2000, **16**(26), 10301–10308.

18 F. F. Rossetti, M. Bally, I. Reviakine, D. Falconnet, R. Michel and M. Textor, Formation of supported phospholipid bilayers on titanium oxide surfaces, *Biophys. J.*, 2005, **88**(1), 7A.

19 M. D. Mager, B. Almquist and N. A. Melosh, Formation and characterization of fluid lipid bilayers on alumina, *Langmuir*, 2008, **24**(22), 12734–12737.

20 K. Dimitrievski and B. Kasemo, Influence of lipid vesicle composition and surface charge density on vesicle adsorption events: a kinetic phase diagram, *Langmuir*, 2009, **25**(16), 8865–8869.

21 C. Satriano, M. Edvardsson, G. Ohlsson, G. Wang, S. Svedhem and B. Kasemo, Plasma oxidized polyhydroxymethylsiloxane—a new smooth surface for supported lipid bilayer formation, *Langmuir*, 2010, **26**(8), 5715–5725.

22 Y. C. Tang, Z. N. Wang, J. W. Xiao, S. H. Yang, Y. J. Wang and P. G. Tong, Studies of phospholipid vesicle deposition/transformation on a polymer surface by dissipative quartz crystal microbalance and atomic force microscopy, *J. Phys. Chem. B*, 2009, **113**(45), 14925–14933.

23 T. M. Bayerl and M. Bloom, Physical properties of single phospholipid bilayers adsorbed to micro glass beads. A new vesicular model system studied by deuterium nuclear magnetic resonance, *Biophys. J.*, 1990, **58**(2), 357–362.

24 D. M. Leneveu, R. P. Rand, V. A. Parsegian and D. Gingell, Measurement and modification of forces between lecithin bilayers, *Biophys. J.*, 1977, **18**(2), 209–230.

25 D. M. Leneveu, R. P. Rand and V. A. Parsegian, Measurement of forces between lecithin bilayers, *Nature*, 1976, **259**(5544), 601–603.

26 J. Radler, H. Strey and E. Sackmann, Phenomenology and kinetics of lipid bilayer spreading on hydrophilic surfaces, *Langmuir*, 1995, **11**(11), 4539–4548.

27 C. F. Lopez, S. O. Nielsen, M. L. Klein and P. B. Moore, Hydrogen bonding structure and dynamics of water at the dimyristoylphosphatidylcholine lipid bilayer surface from a molecular dynamics simulation, *J. Phys. Chem. B*, 2004, **108**(21), 6603–6610.

28 C. H. Hsieh and W. G. Wu, Structure and dynamics of primary hydration shell of phosphatidylcholine bilayers at subzero temperatures, *Biophys. J.*, 1996, **71**(6), 3278–3287.

29 M. J. Higgins, M. Polcik, T. Fukuma, J. E. Sader, Y. Nakayama and S. P. Jarvis, Structured water layers adjacent to biological membranes, *Biophys. J.*, 2006, **91**(7), 2532–2542.

30 M. L. Berkowitz, D. L. Bostick and S. Pandit, Aqueous solutions next to phospholipid membrane surfaces: insights from simulations, *Chem. Rev.*, 2006, **106**(4), 1527–1539.

31 L. Zhang, C. Tian, G. A. Waychunas and Y. R. Shen, Structures and charging of alpha-alumina (0001)/water interfaces studied by sum-frequency vibrational spectroscopy, *J. Am. Chem. Soc.*, 2008, **130**(24), 7686–7694.

32 L. J. Michot, F. Villieras, M. Francois, I. Bihannic, M. Pelletier and J. M. Cases, Water organisation at the solid–aqueous solution interface, *C. R. Geosci.*, 2002, **334**(9), 611–631.

33 S. Jeffery, P. M. Hoffmann, J. B. Pethica, C. Ramanujan, H. O. Ozer and A. Oral, Direct measurement of molecular stiffness and damping in confined water layers, *Phys. Rev. B: Condens. Matter Mater. Phys.*, 2004, **70**(5), 054114(1–8).

34 J. N. Israelachvili, *Intermolecular and Surface Forces*, Academic Press, London, 1985.

35 D. Marsh, *CRC Handbook of Lipid Bilayers*, Boca Raton, FL, 1990.

36 R. K. Iler, *The Chemistry of Silica*, Wiley, New York, 1979.

37 R. R. Madathingal and S. L. Wunder, Effect of particle structure and surface chemistry on PMMA adsorption to silica nanoparticles, *Langmuir*, 2010, **26**(7), 5077–5087.

38 A. L. Troutier, L. Veron, T. Delair, C. Pichot and C. Ladaviere, New insights into self-organization of a model lipid mixture and quantification of its adsorption on spherical polymer particles, *Langmuir*, 2005, **21**(22), 9901–9910.

39 A. D. Petelska and Z. A. Figaszewski, Effect of pH on the interfacial tension of lipid bilayer membrane, *Biophys. J.*, 2000, **78**(2), 812–817.

40 L. T. Zhuravlev, Concentration of hydroxyl-groups on the surface of amorphous silicas, *Langmuir*, 1987, **3**(3), 316–318.

41 Y. Dong, S. V. Pappu and Z. Xu, Detection of local density distribution of isolated silanol groups on planar silica surfaces using nonlinear optical molecular Probes, *Anal. Chem.*, 1998, **70**(22), 4730–4735.

42 R. Tero, H. Watanabe and T. Urisu, Supported phospholipid bilayer formation on hydrophilicity-controlled silicon dioxide surfaces, *Phys. Chem. Chem. Phys.*, 2006, **8**(33), 3885–3894.

43 J. N. Israelachvili and R. M. Pashley, Molecular layering of water at surfaces and origin of repulsive hydration forces, *Nature*, 1983, **306**(5940), 249–250.

44 L. N. Zhang, S. Singh, C. S. Tian, Y. R. Shen, Y. Wu, M. A. Shannon and C. J. Brinker, Nanoporous silica–water interfaces studied by sum-frequency vibrational spectroscopy, *J. Chem. Phys.*, 2009, **130**(15), 154702(1–10).

45 I. M. P. Aarts, A. C. R. Pipino, J. P. M. Hoefnagels, W. M. M. Kessels and M. C. M. van de Sanden, Quasi-ice monolayer on atomically smooth amorphous SiO$_2$ at room temperature observed with a high-finesse optical resonator, *Phys. Rev. Lett.*, 2005, **95**(16), 166104(1–4).

46 V. Ostroverkhov, G. A. Waychunas and Y. R. Shen, Vibrational spectra of water at water/alpha-quartz (0001) interface, *Chem. Phys. Lett.*, 2004, **386**(1–3), 144–148.

47 Q. Du, E. Freysz and Y. R. Shen, Vibrational-spectra of water-molecules at quartz water interfaces, *Phys. Rev. Lett.*, 1994, **72**(2), 238–241.

48 J. Kim, G. Kim and P. S. Cremer, Investigations of water structure at the solid/liquid interface in the presence of supported lipid bilayers by vibrational sum frequency spectroscopy, *Langmuir*, 2001, **17**(23), 7255–7260.

49 H. Kamiya, M. Mitsui, H. Takano and S. Miyazawa, Influence of particle diameter on surface silanol structure, hydration forces, and aggregation behavior of alkoxide-derived silica particles, *J. Am. Ceram. Soc.*, 2000, **83**(2), 287–293.

50 E. A. Vogler, Structure and reactivity of water at biomaterial surfaces, *Adv. Colloid Interface Sci.*, 1998, **74**, 69–117.

51 E. A. Vogler, Water and the acute biological response to surfaces, *J. Biomater. Sci., Polym. Ed.*, 1999, **10**(10), 1015–1045.

52 R. Tero, T. Urisu, H. Okawara and K. Nagayama, Deposition of lipid bilayers on OH-density-controlled silicon dioxide surfaces, *J. Vac. Sci. Technol., A*, 2005, **23**(4), 751–754.

53 *Abstract of papers of ACS*, Aug. 19, 2007, vol. 234, 156-coll.